ADVANCED FUNCTIONAL MATERIALS
www.afm-journal.de

A Flexible Photovoltaic Fatigue Factor for Quantification of Mechanical Device Performance

Lulu Sun, Kenjiro Fukuda, Ruiqi Guo, Luigi A. Castriotta, Karen Forberich, Yinhua Zhou, Takao Someya, Christoph J. Brabec, and Osbel Almora**

Flexible emerging photovoltaic technologies, such as organic and perovskite photovoltaics, hold great potential for integration into tents, wearable electronics, and other portable applications. Recently, Fukuda et al. (2024) propose a bending test protocol for standardizing the mechanical performance characterization of flexible solar cells, focusing on 1% strain over 1 000 bending cycles. This marked an important step toward establishing consistency and good practices in the literature. However, even with this unified protocol, accurately comparing the mechanical flexibility of solar cells is hindered by the variated influence of parameters like thickness, bending radius, and power conversion efficiency (*PCE*) evolution during mechanical testing. Herein, a new figure of merit is introduced, the flexible photovoltaic fatigue factor (*F*), which integrates *PCE* retention, strain, and bending cycles into a cohesive framework. Guided by a detailed multilayer mechanical model, this metric enables more accurate strain analysis and promotes consistent reporting, paving the way for performance optimization in flexible photovoltaics.

1. Introduction

Emerging photovoltaics (ePVs) technologies have garnered significant attention within the research community due to their potential to revolutionize the solar energy market through scalable, cost-effective, and versatile applications.[1] Unlike traditional rigid silicon-based photovoltaics, ePVs offer unique advantages such as flexibility, transparency, and integration into various substrates, making them prime candidates for wearable electronics, curved surfaces, and other unconventional environments.[2] These advancements have paved the way for a new class of applications.[3] However, with this progress comes the necessity to address key challenges, particularly the mechanical and operational stability of these devices when subjected to repetitive mechanical stress.[4]

While power conversion efficiency (*PCE*) remains a critical metric in evaluating the performance of ePV devices, mechanical durability is vital for practical applications.[5] Researchers have comprehensively enhanced the mechanical flexibility of photovoltaic devices from the perspectives of materials, interfaces, and device structure. By modifying molecular design and synthesis, the mechanical properties of semiconductor layers such as polymers and perovskite

L. Sun, K. Fukuda, T. Someya
Thin-Film Device Laboratory
RIKEN
2-1 Hirosawa, Wako, Saitama 351-0198, Japan
E-mail: kenjiro.fukuda@riken.jp
K. Fukuda, R. Guo, T. Someya
RIKEN Center for Emergent Matter Science (CEMS)
2-1 Hirosawa, Wako, Saitama 351-0198, Japan
L. A. Castriotta
Centre for Hybrid and Organic Solar Energy
Electronic Engineering Department
University of Rome Tor Vergata
Via del Politecnico 1, Rome 00118, Italy
K. Forberich, C. J. Brabec
Department of High Throughput Methods in Photovoltaics
Helmholtz Institute Erlangen-Nürnberg for Renewable Energy (HI ERN)
Forschungszentrum Jülich GmbH
Immewahrstraße 2, 91058 Erlangen, Germany
Y. Zhou
Wuhan National Laboratory for Optoelectronics
Huazhong University of Science and Technology
Wuhan 430074, China
T. Someya
Department of Electrical Engineering and Information Systems
The University of Tokyo
7-3-1 Hongo, Bunkyo-ku, Tokyo 113–8656, Japan
C. J. Brabec
Institute of Materials for Electronics and Energy Technology (i-MEET)
Department of Materials Science and Engineering
Friedrich-Alexander-Universität Erlangen-Nürnberg
Martensstraße 7, 91058 Erlangen, Germany
O. Almora
Department of Electronic
Electrical and Automatic Engineering
Universitat Rovira i Virgili
Tarragona 43007, Spain
E-mail: osbel.almora@urv.cat

The ORCID identification number(s) for the author(s) of this article can be found under https://doi.org/10.1002/adfm.202422706

DOI: 10.1002/adfm.202422706

materials have been strengthened, ensuring consistent optoelectronic performance of the photoactive layer under bending conditions.[6] Strategies to enhance interfacial adhesion have also been widely applied in flexible ePVs, preventing delamination and charge carrier extraction degradation after mechanical tests.[7] Additionally, optimizing device structures, such as adopting top-illumination structures and encapsulation materials, effectively mitigates device degradation caused by stress concentration.[8]

Notably, current flexible photovoltaic research predominantly focuses on the retention of *PCE* following mechanical testing, often over hundreds or thousands of bending cycles with different bending radii.[9] Parameters such as bending radius (R) and number of bending cycles (N_{BC}) are frequently reported.[10] For example, the latest reported champion efficiencies on flexible perovskite photovoltaics were reported by Ren et al.[11] and Tong et al.,[12] showing an initial power conversion efficiency ($PCE_{initial}$) value of 25.09 (24.90% certified) and 25.05%, respectively. They reported bending tests with final power conversion efficiency (PCE_{final}) values of 22.58% and 23.29% with relative *PCE* retention (10% and 7% of relative *PCE* lost, respectively) of 90% and 93%, after 10,000 and 5,000 cycles of mechanical bending at radii of 6 and 5 mm, respectively.[11,13] Meanwhile, crucial factors such as substrate thickness, Young's modulus, and layer-by-layer strain distribution are often neglected, which hinders accurate comparisons. For example, even if the same material and device structure are prepared on flexible substrates of different thicknesses, mechanical flexibility will exhibit a large variation due to different stress distributions.[14] The stability of these devices under strain, especially in flexible configurations, has been inconsistent across studies.[15] The absence of standardized testing protocols leads to discrepancies in the reported mechanical stability data, making it difficult to establish clear benchmarks for flexible photovoltaic performance.

Recently, Fukuda et al.[16] proposed a bending test protocol for the mechanical characterization of flexible photovoltaics, recommending 1% strain over 1 000 bending cycles, along with a comprehensible discussion of best practices for mechanical bending methodology and measurement conditions. These values of strain (ϵ) and number of bending cycles (N_{BC}) have been regarded as optimal for the mechanical properties of most typical materials in emerging photovoltaics (see **Table 1**), meaning that bending tests with $\epsilon<1\%$ and N_{BC} <1 000 are likely to provide relatively low stress to the sample.

Literature reports on *PCE* retention in organic photovoltaics (OPV) and perovskite solar cells (PSCs) are plotted in Figure S1 (Supporting Information) and the corresponding data is listed in Table S1 (Supporting Information) as a function of substrate thickness (t_s), ϵ, N_{BC}, and $PCE_{initial}$. We underscore the importance of following best practices, since neglecting parameters such as t_s, ϵ, N_{BC}, and $PCE_{initial}$ hinders the accurate assessment of mechanical performance in flexible photovoltaics. Moreover, while each plot in Figure S1 (Supporting Information) offers valuable insights, a broader view reveals the limitations of *PCE* retention as a standalone metric for assessing mechanical performance. A first take on these plots reveals broadly distributed data, with single high retention values reported for more or less any condition. In a close view, for instance, high *PCE* retention values in Figure S1a (Supporting Information) also show relatively low values of ϵ, and N_{BC} (see Figure S1b,c, Supporting Information), raising questions about whether the devices truly had high performance or simply experienced small mechanical stress during testing. In addition, even though efficiency retention as a function $PCE_{initial}$ in Figure S1d (Supporting Information) shows the final desired outcome, regardless of the bending test, it fails to reflect the mechanical properties of the samples.

In this article, a new figure of merit—the photovoltaic fatigue factor (F)— is proposed as a metric to quantitatively compare the mechanical stability of flexible photovoltaic devices under varying strain and bending cycle conditions. To the best of our knowledge, the proposed fatigue factor is the first single analytical expression that combines essential parameters such as ϵ, N_{BC}, $PCE_{initial}$, and PCE_{final} into a single framework, allowing for more consistent comparisons across different studies and device architectures. This metric is guided by a mechanical strain modeling of the typical multilayer structure of flexible photovoltaic devices. By integrating parameters such as the thickness and Young's modulus of each layer, we provide a comprehensive understanding of how mechanical stress is distributed throughout the device under bending conditions. Using established equations to calculate strain in multilayer stacks, we illustrate the applicability of the photovoltaic fatigue factor in flexible PV technologies, including organic and perovskite solar cells, among others.

2. Revisiting Strain Models in Photovoltaics

Following the common layer structure of ePVs, which includes at least one absorber and two selective transport layers, we consider the bending strain of a multilayer stack with the 1st layer at the bottom and the nth layer at the top (**Figure 1a**).[17] The film thickness and Young's modulus of the ith layer from the bottom (t_i, E_i) determine the strain experienced by the film when bent. In the bent state, the outermost layer (nth layer in Figure 1a) experiences the highest tensile strain in the lateral direction x, whereas the innermost layer (1st layer in Figure 1a) undergoes the highest compressive strain. The strain values vary along the thickness direction (z), with a neutral strain position (b) inside the device, where no strain is applied by bending (Figure 1b). Tensile stresses lead to rupture, while compressive stresses primarily cause delamination (see Figure 1c),[18] and the extent of failure depends on each layer's critical strain and interfacial adhesion. These stresses also affect long-term stability by altering material properties due to the stored strain energy over time.

For example, in flexible OPV devices, understanding the primary degradation mechanisms is crucial for enhancing mechanical and operational stability, especially under repeated flexing and bending. One common degradation issue is the propagation of microcracks within mechanically weak layers, particularly those with lower elasticity or poor adhesion to adjacent layers. These microcracks can initiate under stress and propagate over time, leading to performance degradation through loss of electrical continuity and compromised material integrity. Additionally, accumulated residual stresses are a significant factor in device

Table 1. Young's moduli for materials used in organic solar cells.

Layer	Materials	Young's modulus [Gpa]	Yield strain [%]	Crack onset strain [%]	Reference or remark
Substrate	PDMS	10^{-3}		>100	[18,39]
Substrate	PEN	2–6	6.5–9.6	15–50	[18,24][a]
Substrate	PET	2–5	4–6	30–600	[18,24][b),c)]
Substate	PES	2.5–4.6	3–6.5	40–80	[18,40][d]
Substrate	Colorless polyimide	1.7–4.5	8	100–200	[18][e),f)]
Substrate/encapsulation	Parylene-C	2.8–4	2–3	<200	[18][g]
Substrate/encapsulation	Glass	50–90		0.1[i]	[18][b]
Transparent electrode	ITO	100–150		0.6–1.5	[18,38,41]
Transparent electrode	Graphene	1000		13[i]	[18,42]
Transparent electrode	AgNWs	≤2.64 GPa			[43]
Transparent electrode	Single walled Carbon nanotube	1000		16[i]	[18]
Transparent electrode /Hole transport layer	PEDOT:PSS	0.8–2.8		≈10	[44]
Hole transport layer	MoO_x	90			[4d]
Hole transport layer	Spiro-OMeTAD	15			[45]
Hole transport material	Graphene oxide	208		0.6[j]	[18,46]
Electron transport layer	ZnO	110		0.3[j]	[18,47]
Electron transport layer	TiO_2	230–288			[h]
Electron transport layer	SnO_2	122–304			[48]
Electron transport layer	LiF	65			[i]
Organic active layer	P3HT/PCBM	4.3–6		0.7–2	[49]
Organic active layer	PM6:Y6			5.8	[4b,50]
Organic active layer	PM6:Y7	1.6		2.2	[50–51]
Perovskite active layer	$MAPbI_3$	10–24	1.1–1.7		[52]
Perovskite active layer	$MAPbBr_3$	11–28	0.5–0.6		[52a]
Opaque electrode	Ag	69–83	0.2	50	[18][c]
Opaque electrode	Al	70	2.5—15	0.13–50	[c]
Opaque electrode	Au	77	1–15	30	[7b][c),h)]
Opaque electrode	Cu	110	30	50–60	[7b][c),h)]
Passivation	AlO_x	200–400		≈1	[53][h]
Passivation	SiO_x	66–75		1–4[j]	[h]
Passivation	SiN	166–297		0.5–2[i]	[h]

[a] Teonex, Teijin (https://www.teijin-resin.com/products/teonex); [b] The Engineering ToolBox (https://www.engineeringtoolbox.com/young-modulus-d_417.html); [c] Matweb (https://www.matweb.com/); [d] SUMITOMO CHEMICAL (https://www.sumitomo-chem.co.jp/sep/english/products/pes/pes_fg_ippan.html); [e] Neopulim, Mitsubishi Gas Chemical Company (https://www.mgc.co.jp/eng/products/ac/neopulim.html); [f] PIVAR, Mitsui Chemicals (https://tw.mitsuichemicals.com/rwd1438/store/F2/201202_PIVAR.pdf); [g] Specialty coating systems (https://scscoatings.com/technical-library/); [h] AZO Materials (https://www.azom.com/); [i] CRYSTRAN (https://www.crystran.co.uk/optical-materials/lithium-fluoride-lif); [j] It is unclear from the literature whether COS or yield strain values are shown.

degradation. These stresses can arise from repeated mechanical deformation or temperature changes and are often exacerbated by mismatches in Poisson's ratios between different layers. These mismatches might lead to differential expansion or contraction, creating concentrated stress points with microstructural failures, such as delamination or cracking at the interfaces. To mitigate these issues, multilayer designs or stress-buffering layers can help absorb and/or redistribute stresses throughout the device. Moreover, exploring materials with compatible mechanical properties, especially in terms of Poisson's ratio and Young's modulus, could reduce the buildup of residual stresses. Such strategies are essential for extending the operational life and reliability of flexible PVs, particularly in applications demanding extensive bending or exposure to dynamic environments.

Since degradation and failure of devices are typically governed by strain imposed on the material, discussing strain (instead of the bending radius) is critical at the fundamental research level. In the following sections, we will discuss how to calculate strain experienced by individual flexible films having multi-stack configurations.

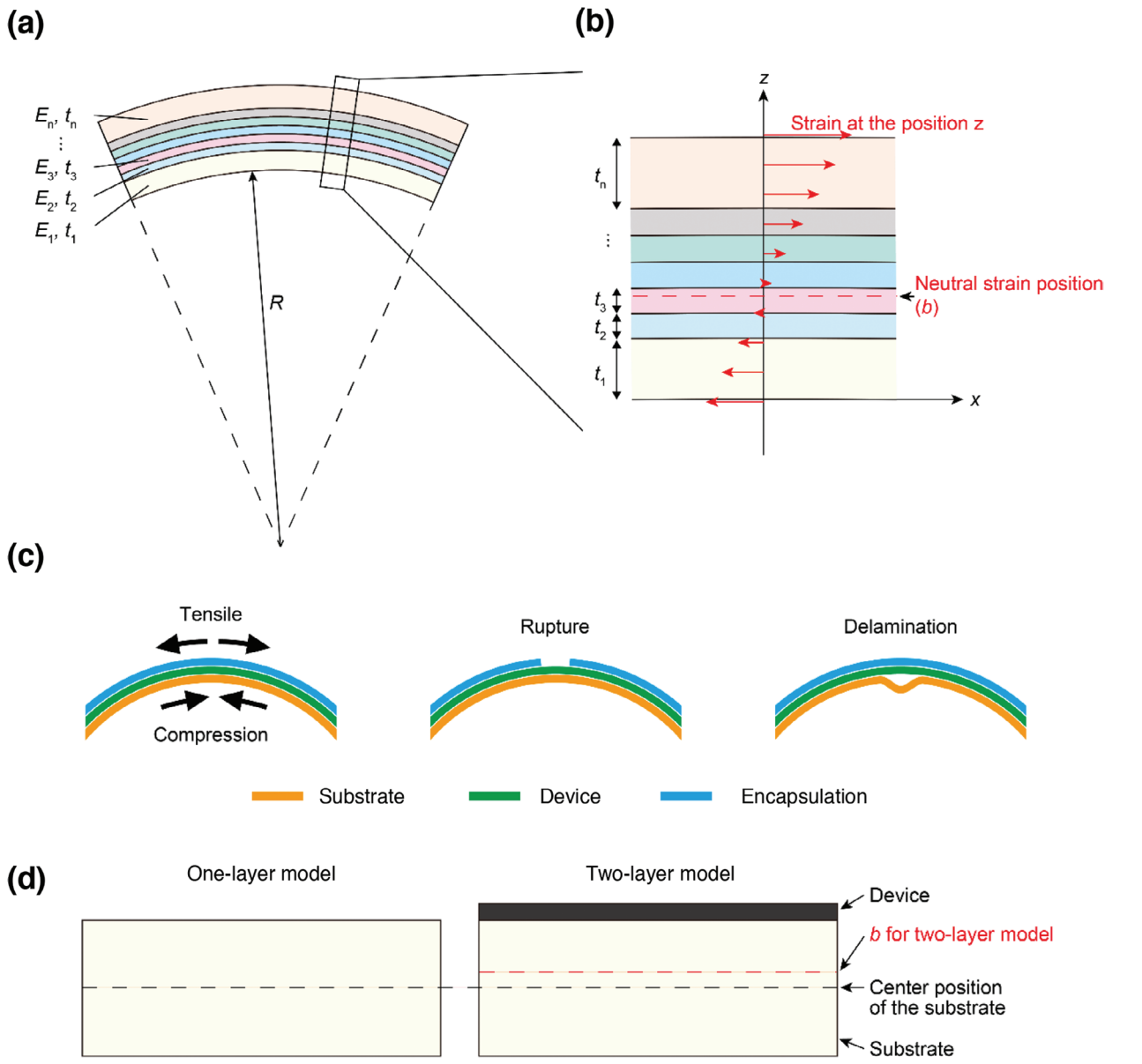

Figure 1. Schematic of multilayer stacks for strain mechanical models. The cross-section view used to denote the neutral mechanical plane in a) is magnified in b). In c), a schematic illustration illustrates the typical failure of a device with a multi-stack structure under applied bending strain. d) Schematic of the one-layer and the two-layer models. The neutral strain position *b* shifts from the center of the substrate toward the device side due to the thin device placed on the substrate.

The equation for bending strain of a multilayer stack ϵ_{ML} in the lateral direction (x) at any position along the thickness (z) is given by:[17]

$$\epsilon_{ML} = \frac{z - b}{R} \tag{1}$$

where R is the bending radius and b is the neutral mechanical plane (zero-strain position) given by:[19]

$$b = \frac{\sum_{i=1}^{n} E_i t_i \left[\sum_{j=1}^{i} t_j - \frac{t_i}{2}\right]}{\sum_{i=1}^{n} E_i t_i} \tag{2}$$

where E_i and t_i denote the Young's moduli and thicknesses of the individual layers. Equation (1) shows that ϵ_{ML} becomes 0 at the position $z = b$. The strain has a negative value below the neutral mechanical plane and a positive value above it. Since we are considering outward bending here, positive values correspond to a tensile strain (z equals the total thickness in Equation (1)), and negative values correspond to compressive strain ($z = 0$ in Equation (1)). The maximum tensile strain is applied at the top surface, and the minimum (absolute maximum) compressive strain is applied at the bottom surface. In the real operation of flexible devices, both outward (positive) and inward (negative) bending may be experienced.[20] However, we conveniently recommend

outward bending for mechanical performance comparisons[16] taking the absolute value of the strain, with the substrate as the 1st layer and the device layer(s) at the nth position.

Since Equations (1) and (2) complicate obtaining strain values, many reports use approximations to calculate the strain under bending. Here, we will discuss the assumptions made in these approximations and their validity. When $n = 1$ in Equation (2), the bending strain of a single and uniform material will be considered. In this case, the neutral mechanical plane of such single-layer film b_{1L} is given by:

$$b_{1L} = \frac{E_1 t_1 \left(\frac{t_1}{2}\right)}{E_1 t_1} = \frac{t_1}{2} \tag{3}$$

Then, the lateral strain (ε_{1L}) can be determined by the following equation:

$$\varepsilon_{1L} = \frac{z - \frac{t_1}{2}}{R} \tag{4}$$

Therefore, the maximum strain at the top surface ($z = t_1/2$) is given by:

$$\varepsilon_{1L} = \frac{t_1}{2R} \tag{5}$$

Notably, Equations (1–5) are applicable to both inward and outward bending cases, providing the corresponding strain value sign and numbering for the layers in Equation (1). For instance, for inward bending in Equation (1), the device starts at the 1st layer and the substrate becomes the nth layer.

The one-layer model in Equation (5) can conveniently describe the strain in thin-film solar cells taking t_1 as the thickness of the substrate when the mechanical properties of the actual "device" do not contribute significantly. However, this is not always the case. Typical flexible PVs use a multilayer stack structure, and the relation between the thicknesses and Young's moduli of each layer can affect the strain.

As an alternative to Equation (5), the most frequently used approach is to simplify the multilayer stack to two layers: a thick substrate with thickness t_s and Young's modulus E_s and a uniform "device" layer with thickness t_d and Young's modulus E_d. In this case, the first and second layers correspond to the substrate and the device, respectively ($t_1 = t_s$, $E_1 = E_s$, $t_2 = t_d$, $E_2 = E_d$). For these two-layer cases, the neutral position b_{2L} can be obtained as follows by setting $n = 2$ in Equation (2):

$$b_{2L} = \frac{E_1 t_1 \left(\frac{t_1}{2}\right) + E_2 t_2 \left(t_1 + \frac{t_2}{2}\right)}{E_1 t_1 + E_2 t_2} = \frac{t_1}{2} \frac{1 + 2\frac{E_2}{E_1}\frac{t_2}{t_1} + \frac{E_2}{E_1}\left(\frac{t_2}{t_1}\right)^2}{1 + \frac{E_2}{E_1}\frac{t_2}{t_1}} \tag{6}$$

Here, by using the new parameters $\eta = t_d/t_s$ and $\chi = E_d/E_s$ representing the ratios of thickness and Young's modulus, respectively, Equation 6 can be rearranged to:[21]

$$b_{2L} = \frac{t_s}{2} \frac{1 + \chi\eta(2 + \eta)}{1 + \chi\eta} = \frac{t_s}{2} \frac{1 + 2\chi\eta + \chi\eta^2}{1 + \chi\eta} \tag{7}$$

In this case, the neutral strain position b_{2L} shifts from the center of the substrate toward the device side due to the device being placed on the substrate (Figure 1d). The position at the top surface (or surface of the device) can be expressed as $z = t_s + t_d$, thereby the two-layer tensile strain at the top surface in outward bending is given by:

$$\varepsilon_{2L} = \frac{t_s + t_d - b_{2L}}{R} = \frac{t_s}{2R} \frac{1 + 2\eta + \chi\eta^2}{1 + \chi\eta} \tag{8}$$

If Young's moduli of the substrate and the device are similar and the device thickness is much smaller than that of the substrate ($t_d \ll t_s$ or $\eta = 0$), Equation (8) can be simplified to the one-layer model of Equation (5); i.e. $\varepsilon_{2L} \cong \varepsilon_{1L}$.[20] In cases where the above approximation is valid, we can use the simpler Equation (5) for the strain calculations.

The simple one-layer strain model introduced in Equation (5) provides a good description for devices that behave as a simple effective material, which is a valid approximation when the mechanical properties of all layers are similar. We conducted mechanical simulations (COMSOL Multiphysics, see section S1, Supporting Information) to examine the impact of varying substrate thickness on the stress distribution, as shown in **Figure 2a**. The simulation results clearly demonstrate that increasing substrate thickness proportionally raises stress for a given device thickness, significantly affecting their mechanical performance. Equation (5) illustrates the important point that the thinner the film, the smaller the value of strain imposed on the surface for the same radius of curvature (Figure 2b). This has been experimentally demonstrated by recent reports of "clumpable" photovoltaics using substrates with a thickness on the order of 1 µm.[2a,8a,22] The equation shows the importance of specifying the thickness of the substrate (and other layers) for a fair comparison of flexibility properties among different devices.

Furthermore, we discuss the appropriate range of the approximation that calculates the strain of a multilayered device using a simplified one-layer model by comparing the one-layer model with a two-layer model. In the two-layer model, the strain under a specific bending radius depends on both the ratio of thicknesses η and the ratio of Young's moduli χ. We have plotted the radius of curvature for $\varepsilon_{2L} = 1\%$ under the constraint of a fixed device thickness of 1 µm (Figure 2c,d).[18] As in the one-layer model, it is observed that the smaller the thickness of the substrate (that is, the larger the η), the smaller the value of the radius of curvature that gives $\varepsilon = 1\%$ strain. In addition, this plot suggests another important correlation with respect to χ. Specifically, the larger the value of χ (indicating softer substrates in relation to the device), the smaller the value of the radius of curvature that gives $\varepsilon_{2L} = 1\%$ strain. This implies that employing an extremely soft substrate is an effective engineering approach to improve the bending cycle stability at the same curvature radius. This is exemplified in the research conducted on OPVs by Cui *et al.*,[23] utilizing polydimethylsiloxane (PDMS) soft elastomer material as substrates.

The distribution of $\varepsilon_{2L}/\varepsilon_{1L}$ is plotted versus thickness ratio η and Young's moduli ratio χ in Figure 2e. In the ranges where $\eta < 0.1$ and $\chi < 10$, both models are nearly equivalent ($\varepsilon_{2L} \cong \varepsilon_{1L}$). On the other hand, the one-layer model underestimates the strain ($\varepsilon_{2L} \geq 2\varepsilon_{1L}$) for $\eta > 0.5$ and $\chi < 1$, and overestimates it

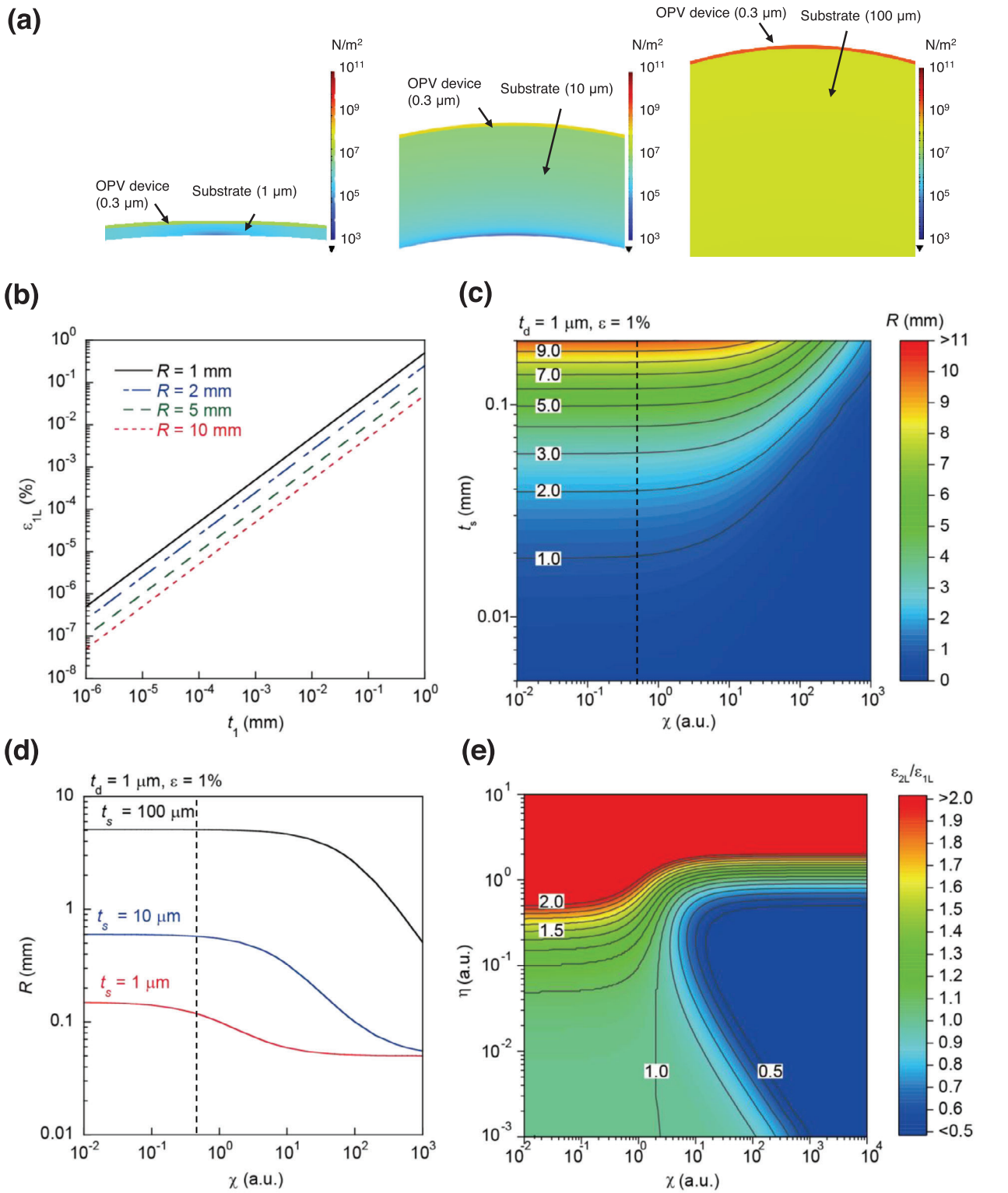

Figure 2. One-layer and two-layer strain models simulation. a) Mechanical stress simulations of OPV devices on substrates of different thicknesses (1, 10, and 100 μm) under bending. b) Absolute strain calculated according to the one-layer model of Equation (5) as a function of the film thickness t_1 and for different bending radii. c,d) Bending radius in the two-layer model calculated using Equation (8). The black dashed line indicates Young's modulus of the typical substrate (PET) of the flexible PVs. The contour plot (c) considers a film with $\varepsilon_{2L} =$ 1% on a device thickness (t_d) of 1 μm versus Young's modulus ratio $\chi = E_d / E_s$ and substrate thickness t_s. The 2D graph d) plots the corresponding bending radius curves as a function of χ for three t_s values: 100 μm (black), 10 μm (blue), and 1 μm (red). e) Comparison of strain values calculated with the two-layer model (ε_{2L}) and the one-layer model (ε_{1L}). The color represents the strain ratio $\varepsilon_{2L}/\varepsilon_{1L}$ depending on the thickness ratio $\eta = t_d / t_s$ and Young's modulus ratio $\chi = E_d / E_s$.

($\varepsilon_{2L} \leq \varepsilon_{1L}/2$) for $\chi > 100$. Common substrate materials in flexible ePVs are polyethylene naphthalate (PEN) or polyethylene terephthalate (PET), with a typical thickness of 100 µm and a Young's modulus of units of GPa.[18,24] With a typical device thickness in the order of 1 µm, and the largest Young's modulus in the device of ≈100 GPa for metal oxides such as indium-tin-oxide (ITO),[18] such a condition gives $\eta = 0.01$ and $\chi = 10$, which are within the range that both models are nearly equivalent ($\varepsilon_{2L} \cong \varepsilon_{1L}$). Therefore, using the approximation of the simplest model is reasonable. However, if the elastic properties and/or the film thickness ratios of more than one layer are outside the range discussed above, simple strain calculations using the one-layer or two-layer approximations are likely to be inappropriate. In such cases when the substrate is very thin (typically < 10 µm) or extremely soft (using materials over 100 times softer than the electrodes), it is more accurate to calculate strain using the multilayer model, using the thickness and Young's modulus of each layer as input parameters. Experimentally, determining Young's moduli for multilayer films can be challenging. Therefore, literature values or similar values from comparable materials can be used as approximations. Alternatively, a range approximation can be done for the two-layer model with respect to Young's moduli. The minimum strain in the two-layer model is found when $E_d \gg E_s$ in Equation (8), i.e. $\lim_{\chi \to \infty} \varepsilon_{2L}$, which results

$$\varepsilon_{2L,min} = \frac{t_s}{2R}\eta = \frac{t_d}{2R} \tag{9}$$

Note that Equation (9) leads to the one-layer model of Equation (5), only that $t_d = t_1$ indicates a much softer composition of the substrate (below in Figure 1d) with respect to the device (above in Figure 1d). On the other hand, the maximum strain in the two-layer model is found when $E_d \ll E_s$ in Equation (8), i.e. $\lim_{\chi \to 0} \varepsilon_{2L}$, leading to

$$\varepsilon_{2L,max} = \frac{t_s}{2R}(1 + 2\eta) = \frac{t_s + 2t_d}{2R} \tag{10}$$

Equation (10) indicates that the thickness of a much softer device layer (above in Figure 1d), can contribute up to twice the strain value than the thickness of the substrate (below in Figure 1d). The strains of Equations (9 and 10) provide a range for $[\varepsilon_{2L,min},\ \varepsilon_{2L,max}]$ where the experimental strain could be expected, which can be used for comparison. In addition, note that Equations (8–10) correspond to the outward tensile bending case, following recent guidelines recommendations.[16] Other strain configurations would require different analytical or numerical approaches for estimating the strain. Typical examples include: inward compressive bending, near-neutral strain bending in encapsulated flexible solar cells, and stretching.

In summary, the multilayer model provides greater accuracy than the single-layer model when considering extremely thin or soft materials as substrates. Soft elastomer substrates such as PDMS and thin substrates with thicknesses of ≈1 µm, are typical examples where the multilayer model is essential. For instance, a single 1 µm-thick substrate film requires a bending radius of $R = 50$ µm to generate a 1% strain at the outermost surface. Mainstream devices, however, typically use 100 µm PEN/PET substrates. When such substrates, along with functional layers totaling 1 µm or less in thickness, are used in ePV structures, the difference between ε_{1L} and ε_{ML} becomes negligible and using ε_{1L} is acceptable. For example, a 5 mm bending radius to a 100 µm substrate results in a 1% strain in the single-layer strain model (Figure 2b). Table 1 outlines Young's moduli of commonly used materials for flexible ePV devices. It is critical to clearly specify the substrate thickness and, when possible, provide cross-sectional images showing the thickness of each layer. This clarity ensures accurate strain analysis and validates the strain calculations.

Overall, bending test evaluations for flexible photovoltaics should prioritize applied strain over bending radius alone. Substrate thickness is a crucial factor in determining strain values, and it is important to explicitly report both the total device thickness and individual layer thicknesses. For polymer substrates thicker than 10 µm with Young's modulus ≈1 GPa, a simple strain calculation using Equation (5) is generally sufficient. This applies to most of the reported flexible organic photovoltaics which currently use plastic substrates thicker than 100 µm, while devices are thinner than 1 µm. However, strain calculations using more rigorous equations (Equation (1), (2), and (8)) are recommended when discussing ultrathin and highly soft substrates. In these cases, two or more layers should be accounted for the evaluation of the strain.

3. The Flexible Photovoltaic Fatigue Factor for Solar Cells

When similar mechanical tests use the same strain and cycle numbers, instead of the bending radius, it becomes relatively easy to make a fair comparison between multiple literature results. However, when the values of ε and/or N_{BC} are different, it may be unclear whether the mechanical stability test results are due to the measurement method or the sample properties. In this case, an appropriate parameter for accurate and objective comparison should be considered accounting for both the mechanical and photovoltaic performance of solar cells in bending tests. Accordingly, we propose a first-time analytical expression for the flexible photovoltaics fatigue factor:

$$F = \frac{\Delta PCE}{PCE_{initial} \cdot \varepsilon \cdot \log_{10}\left[N_{BC}\right]} \tag{11}$$

where $\Delta PCE = PCE_{final} - PCE_{initial}$ is the power conversion efficiency difference between the value before ($PCE_{initial}$) and the one (PCE_{final}) after a number of bending cycles (N_{BC}) in a mechanical stability test with a given absolute value strain (ε) to the device. Notably, the value of ε can be estimated using Equations (5) or (8), which serve as good tensile strain approximations for the one-layer and the two-layer models, respectively. These models are applicable to most common thin-film flexible solar cells. However, for devices where the mechanical and geometrical properties of the layer sequence cannot be simplified to a single "device layer," the strain formulation using Equations (1) and (2) must be redefined. In such cases, ε and F should be explicitly referenced with respect to a specific layer within the device, such as the absorber layer. Additionally, while ε and N_{BC} can theoretically take any positive values, we recommend conducting experiments with

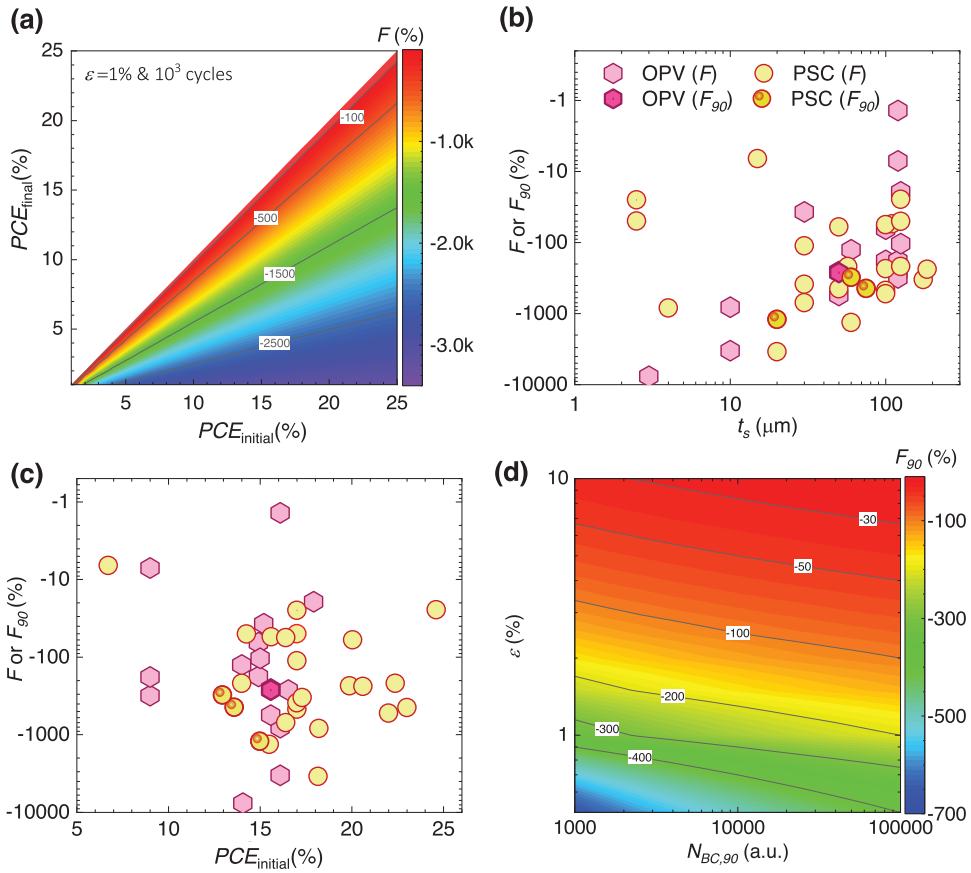

Figure 3. Flexible photovoltaic device fatigue factor. Panel a) shows calculated F values for 1% strain and 1000 bending cycles within the range up to 25% *PCE* in Equation (11); b,c) show experimental values from the literature, as summarized in Table S1 (Supporting Information), as a function of the substrate thickness and initial power conversion efficiency; d) shows the simulated values for F_{90} following Equation (12).

$\varepsilon = 1\%$ and $N_{BC} = 1000$ as baseline conditions for consistency and comparability.[16]

The newly introduced definition (11) is expressed as a percentage, the fatigue factor indicates how different the mechanical performance of the device is with respect to a reference device with unitary fatigue factor $F = -1$ (e.g., 1% decrease of *PCE* after 10 bending cycles with 1% strain). For example, **Figure 3**a shows the calculated values for F as a function of the initial and final efficiencies, assuming $\varepsilon = 1\%$ and $N_{BC} = 1000$ in Equation (11). In that plot, it is clear that small percentages of F require high *PCE* stability under higher bending cycles tests. Particularly, the $\log_{10}[N_{BC}]$ dependency of F was introduced in analogy with typical experimental behaviors for stress-cycles curves in polymers[25] and steel,[26] and because of practical reasons, for avoiding ambiguity in F from tests with low strain and high number of cycles.

The value of F is determined by the mechanical and photovoltaic properties of the materials comprising the flexible solar cells. Mechanically, the strain provides the information on structure, geometry and Young's modulus. Additionally, the bending radius within the strain offers a relative measure on how close the material is to its respective yield strain and crack onset strain. From a photovoltaic perspective, the properties of the active device materials directly influence ΔPCE. For instance, even if the cell architecture is optimized to position the active device layers at a neutral strain location, variations in F would be expected due to differences in the optoelectronic properties of the device materials. Furthermore, the dependency of ε and ΔPCE on N_{BC} highlights how both mechanical and photovoltaic material properties collectively impact cell performance during bending tests, ultimately shaping the value of F.

Intuitively, a greater sample instability correlates with higher absolute values of $|F|$, with a negative sign indicating a decrease of *PCE*. Conversely, a high stability of flexible cells would correspond to small absolute values of $|F|$. Positive values of F denote an increase in *PCE*, while negative values signify a decrease. Note that ε is recommended positive,[16] from outward tensile strain bending, but F is defined in Equation (11) as a function of the absolute value of ε for avoiding sign ambiguity (e.g., with inward bending). Therefore, the sign of F should only indicate that of ΔPCE. Moreover, although $F < 0$ is more typical and generally expected for bending tests with high values of ε and N_{BC}, positive values ($F > 0$) can be often observed for intermediate and low values of ε and N_{BC}. This latter scenario aligns with the characteristic initial increase in *PCE* observed in early stages of stability tests in emerging PV technologies such as PSCs.[27] However, for other PV technologies or for bending tests conducted under high values of ε and N_{BC}, the definition of F can be simplified

to its absolute form, to more intuitively represent performance losses: the smaller the value of $|F|$, the better.

The fatigue factor $F(PCE_{final})$ takes the "least desired" value when full PCE degradation ($PCE_{final} = 0$, 0% PCE retention) occurs, namely $F = -1/\varepsilon \ \mathrm{Log}_{10}[N_{BC}]$. For instance, when comparing two cells until complete PCE decrease under the same 1% strain, the higher the bending cycles the better the performance of the device, resulting in a higher F value (smaller $|F|$ absolute value).

In contrast, the optimum outcome from an operational and mechanical stability test would be the complete stability ($PCE_{final} = PCE_{initial}$, 100% PCE retention) making $F = 0$; i.e. no fatigue. Using an analogy, water freezing point (0 °C) is to temperature T what complete stability (0%) is to fatigue factor F. Nevertheless, care must be taken with reporting experimental values of $F = 0$, which neglects the experimental accuracy of the bending test and prevents the comparison between samples with similar PCE steadiness but different measurement conditions.

For example, neglecting experimental accuracy results in $F = 0\%$ for two different cells with $PCE_{final} = PCE_{initial} = 10.0\%$ tested under 1% strain, after 1000 and 10000 bending cycles, respectively, despite the fact that the performance is better for the cell with the higher value of N_{BC}. This problem can be solved by, for instance, using a one-digit ΔPCE for the last specified significant digit of the PCE values. Accordingly, the aforementioned example ($PCE_{final} = PCE_{initial} = 10.0 \pm 0.1\%$) can be solved taking $PCE_{final} \approx 9.9\%$ in both samples, which results in $\Delta PCE = -0.1\%$ and different values of $F = -0.33$ and $F = -0.25$ for the cells with 1000 and 10000 bending cycles, respectively. This approximation clearly expresses the different performances of each device and allows for a more accurate comparison.

Experimental values for F have been calculated for mechanical stability tests reported in the literature, as listed in Table S1 (Supporting Information). The results are displayed in Figure 3b,c as a function of the substrate thickness and the initial efficiency, respectively. In these plots, the best-performing reports are expected toward the top region of the graphs, i.e. highest F values (smallest absolute values $|F|$). Notably, the graph in Figure 3b separates the behavior of ultra-thin devices from more typical samples based on the thicker devices. Moreover, the graph of Figure 3c focuses on efficiency, showing the most desired outcomes toward the right-top region of the plot. The highest values for F are found for OPV cells, whereas the lowest substrate thicknesses and highest PCE values correspond to PSCs, as presented in Figure 3b,c.

Illustratively, Figure S2 (Supporting Information) presents simulated F values for $\Delta PCE = -0.01\%$, 1% strain and several numbers of bending cycles as a function of the bandgap energy assuming $PCE_{initial}$ as the detailed balance efficiency limit for single junction solar cells.[54] Notably, these values do not express a physical dependency of F on the bandgap of the materials, but a mathematical consequence of the measurement accuracy selected for ΔPCE. Nevertheless, a clear indication is shown that the higher the initial efficiency, the better.

The best experimental value for the fatigue factor has been found for the devices reported by Qin *et al.*,[28] with $F = -1.38\%$ for a PM6:BTP-eC9:$PC_{71}BM$-based flexible OPV cell on a 120 µm-thick PET(Ag-grid) substrate tested over 1000 bending cycles under 1.5% strain. Furthermore, among PSCs, the highest mechanical stability with $F = -6.61\%$ has been achieved by Ahn *et al.*,[29] who fabricated a $MAPbI_3$-based cell on a PEI substrate with a thickness of 15 µm, tested during 1000 bending cycles under a 0.75% strain, although the initial efficiency of these samples (6.72%) was relatively low. Moreover, we also highlight the work by Tan *et al.*,[7d] who reported flexible all-perovskite tandem solar cells with a substrate thickness of 175 µm and $PCE_{initial} = -24.6\%$ that withstood 10 000 bending cycles with $R = 15$ mm for $\varepsilon = 0.58\%$ without degradation (100% PCE retention). Considering the reported accuracy, $\Delta PCE = -0.1\%$ leads to $F = -17.4\%$ for the tandem cell.

The definition of flexible photovoltaic fatigue factor in Equation (11) can be understood as a function $F(\varepsilon, N_{BC}, X_{initial}, X_{final})$, where the performance parameter X is the PCE. In a more generalized approach, X could refer to the evolution of other performance parameters (e.g., V_{oc}, J_{sc}, FF) before and after the mechanical bending test. Moreover, even though the in situ tracking of performance parameters may be experimentally challenging during bending tests, the fatigue factor could also be represented as a function of the number of bending cycles, i.e., $F(\epsilon, X(N_{BC}))$. Therefore, one could focus on the evolution of the performance parameter up to un specific percentage of decrease/retention. For example, for $PCE_{final}/PCE_{initial} = 0.9$ we could define

$$F_{90} = -\frac{1}{10 \cdot \varepsilon \cdot \log_{10}\left[N_{BC90}\right]} \tag{12}$$

where F_{90} is the fatigue factor for the PCE to reach 90% of the initial value after a number of bending cycles N_{BC90}. Illustratively, Figure 3b displays some experimental F_{90} values reported in the literature, although the corresponding data does not relate to the in situ measurement of $PCE(N_{BC})$.

Figure 3d shows the simulated values of F_{90} for strains ranging from $0.5\% < \varepsilon < 10\%$ and cycle counts $10^3 < N_{BC90} < 10^5$. This plot illustrates that, for an equivalent relative decrease in PCE, higher strain and/or a greater number of bending cycles lead to a higher fatigue factor (indicated by a smaller absolute value $|F_{90}|$, reflecting lower stability). The metric F_{90} proves particularly useful in bending tests with high values of ε and small values of N_{BC}. For example, in a test where a solar cell is bent ten times ($N_{BC} = 10$) between each $J-V$ curve measurement, a small ε might result in negligible PCE loss, necessitating a large number of cycles or continuous bending, which can be time-consuming. Instead, by incrementally increasing strain (e.g., reducing the bending radius) every ten cycles, the $J-V$ curve could be measured until the PCE retention is 90% for $N_{BC90} = 10$. This approach not only conserves time but also provides valuable information on yield and crack-onset strains, potentially reducing the need for extensive bending equipment.

The definition in Equation (12) can also be generalized as $F_{\%}(\epsilon, X(N_{BC\%}))$ where, the flexible fatigue factor $F_{\%}$ is calculated for the number of bending cycles $N_{BC\%}$ that results in a specified percentage decrease "%" of the parameter X, during a bending test at strain ε. For instance, in PV devices, X could represent other performance metrics from the $J-V$ curves, such as V_{oc}, J_{sc}, FF, or alternative properties derived from different characterization techniques conducted before, after, or during the bending test. Importantly, this approach could further be extended to

other flexible energy devices, such as capacitors,[30] batteries,[31] thermoelectrics,[32] magnetocalorics,[33] and piezoelectronics,[34] where X could be suitably redefined to align with the performance attributes relevant to each device.

Importantly, limitations can also be argued with respect to the definition of F, which requires careful consideration. F is directly proportional to the decrease in photovoltaic output power ($\Delta P_{out} \propto \Delta PCE$), which is influenced by several test parameters, such as temperature, incident photon flux, bias, and test duration. Specifically, test duration and bending rate (or frequency) are related to the strain power, which is proportional to the square root of the strain. Therefore, one could argue that F would benefit from incorporating a factor proportional to these parameters, to reflect the energy ratio between the operational photovoltaic output and strain energy.

At the core of F's definition is the relative damage applied during the bending test (see e.g., Miner's damage rule) which is put into perspective with the photovoltaic performance for the first time.[35] This relates to the need to evaluate the PCE behavior in terms of the stress–strain and stress cycle curves.[36] These curves illustrate how closely the test values of ϵ and N_{BC} are with respect to those corresponding to the yield strength[37] and crack onset[38] values, with proximity indicating greater damage (decreasing PCE) and a more extreme test. However, even though the expression of F could also benefit from including a mechanical damage factor dependency, its definition in Equation (11) effectively captures and compares the photovoltaic mechanical performance in practical applications. This highlights the need for detailed reporting of mechanical and operational tests and points to critical research directions, such as exploring the relationships between photovoltaic fatigue and mechanical damage, bending frequency, temperature, yield strain, and crack onset strain.

4. Conclusion

In this article, a new figure of merit is introduced: the flexible photovoltaic fatigue factor F for solar cells, which condenses the operational decay over bending cycles for a given strain condition. In the definition of F, we highlight the importance of accurate estimation of ϵ, which summarizes the information on the mechanical stress applied to the flexible solar cell during the bending test, while ΔPCE expresses the photovoltaic performance stability over bending cycles. Particularly, for in situ mechanical and operational stability tests, the F_{90} fatigue factor is also proposed which is related to the number of bending cycles for which a 90% reduction of the power conversion efficiency is found.

We encourage the best practices in the characterization of the mechanical performance of flexible solar cells, following the bending test protocol proposed by Fukuda et al., and underscore the importance of a detailed description of the experiments and strain calculation models. Specifically, we strongly recommend reporting the values of t_s, R, ϵ, $N_{BC,}$ $PCE_{initial}$, and PCE_{final}. By adopting such standardized reporting practices and utilizing the fatigue factor as a universal metric, the field of flexible photovoltaics can move toward a more consistent and comparable framework for assessing mechanical stability. Our work provides a practical tool for researchers and lays the groundwork for future developments in the design and optimization of flexible photovoltaic systems for real-world applications.

Additionally, we highlight that while this first formulation of the analytical expression for F is both effective and practical for the majority of common flexible solar cells to date, the future development of non-rigid solar cells may necessitate alternative bending tests and more sophisticated analytical approaches for estimating ϵ. For instance, inward bending, near-neutral stress bending in encapsulated cells, and stretching tests could even require the introduction of new parameters analogous to F to account for the unique mechanical and photovoltaic behaviors of such devices.

Supporting Information

Supporting Information is available from the Wiley Online Library or from the author.

Acknowledgements

This study was supported by the Japan Society for the Promotion of Science under Grants-in-Aid for Scientific Research (S) (No. JP22H04949). K.F. acknowledges the support from JST ASPIRE for Rising Scientists (JPMJAP2336). O.A. acknowledges the Juan de la Cierva Fellowship grant FJC2021-046887-I funded by MICIU/AEI/ 10.13039/501100011033 and by the European Union NextGenerationEU/PRTR. K.F. acknowledges support by the Helmholtz Association in the framework of the innovation platform "Solar TAP". L.A.C. acknowledges the European Union's Framework Programme for Research and Innovation Horizon Europe (2021-2027) under the MarieSkłodowska-Curie Grant Agreement No. 101068387 "EFESO".

Conflict of Interest

The authors declare no conflict of interest.

Keywords

bending test, flexible solar cells, mechanical stability, mechanical strain, operational photovoltaic stability

Received: November 21, 2024
Revised: December 16, 2024
Published online: January 5, 2025

[1] a) R. Liu, Z. L. Wang, K. Fukuda, T. Someya, *Nat. Rev. Mater.* **2022**, *7*, 870; b) Y. Li, X. Huang, H. K. M. Sheriff, S. R. Forrest, *Nat. Rev. Mater.* **2023**, *8*, 186; c) N.-G. Park, K. Zhu, *Nat. Rev. Mater.* **2020**, *5*, 333; d) C. Yan, S. Barlow, Z. Wang, H. Yan, A. K. Y. Jen, S. R. Marder, X. Zhan, *Nat. Rev. Mater.* **2018**, *3*, 18003.

[2] a) M. Kaltenbrunner, M. S. White, E. D. Głowacki, T. Sekitani, T. Someya, N. S. Sariciftci, S. Bauer, *Nat. Commun.* **2012**, *3*, 770; b) B. Hailegnaw, S. Demchyshyn, C. Putz, L. E. Lehner, F. Mayr, D. Schiller, R. Pruckner, M. Cobet, D. Ziss, T. M. Krieger, A. Rastelli, N. S. Sariciftci, M. C. Scharber, M. Kaltenbrunner, *Nat. Energy* **2024**, *9*, 677; c) D. Lv, Q. Jiang, Y. Shang, D. Liu, *npj Flex. Electron.* **2022**, *6*, 38; d) L. Sun, W. Zeng, C. Xie, L. Hu, X. Dong, F. Qin, W. Wang, T. Liu, X. Jiang, Y. Jiang, *Adv. Mater.* **2020**, *32*, 1907840; e) Y. Zhang, S.-W. Ng, X. Lu, Z. Zheng, *Chem. Rev.* **2020**, *120*, 2049.

[3] J.-H. Lee, K. Cho, J.-K. Kim, *Adv. Mater.* **2024**, *36*, 2310505.

[4] a) M. Kaltenbrunner, G. Adam, E. D. Głowacki, M. Drack, R. Schwödiauer, L. Leonat, D. H. Apaydin, H. Groiss, M. C. Scharber, M. S. White, N. S. Sariciftci, S. Bauer, *Nat. Mater.* **2015**, *14*, 1032; b) J. Han, F. Bao, D. Huang, X. Wang, C. Yang, R. Yang, X. Jian, J. Wang, X. Bao, J. Chu, *Adv. Funct. Mater.* **2020**, *30*, 2003654; c) R. Miao, P. Li, W. Zhang, X. Feng, L. Qian, J. Fang, W. Song, W. Wang, *Adv. Mater. Interfaces* **2022**, *9*, 2101669; d) W. Huang, Z. Jiang, K. Fukuda, X. Jiao, C. R. McNeill, T. Yokota, T. Someya, *Joule* **2020**, *4*, 128.

[5] a) L. Zhu, M. Zhang, Z. Zhou, W. Zhong, T. Hao, S. Xu, R. Zeng, J. Zhuang, X. Xue, H. Jing, Y. Zhang, F. Liu, *Nat. Rev. Electr. Eng.* **2024**, https://doi.org/10.1038/s44287-024-00080-3; b) J. Hou, O. Inganäs, R. H. Friend, F. Gao, *Nat. Mater.* **2018**, *17*, 119; c) J. Y. Kim, J.-W. Lee, H. S. Jung, H. Shin, N.-G. Park, *Chem. Rev.* **2020**, *120*, 7867; d) K. O. Brinkmann, P. Wang, F. Lang, W. Li, X. Guo, F. Zimmermann, S. Olthof, D. Neher, Y. Hou, M. Stolterfoht, T. Wang, A. B. Djurišić, T. Riedl, *Nat. Rev. Mater.* **2024**, *9*, 202.

[6] a) E. Dauzon, X. Sallenave, C. Plesse, F. Goubard, A. Amassian, T. D. Anthopoulos, *Adv. Mater.* **2021**, *33*, 2101469; b) J. S. Park, G.-U. Kim, S. Lee, J.-W. Lee, S. Li, J.-Y. Lee, B. J. Kim, *Adv. Mater.* **2022**, *34*, 2201623; c) X. Li, H. Yu, Z. Liu, J. Huang, X. Ma, Y. Liu, Q. Sun, L. Dai, S. Ahmad, Y. Shen, M. Wang, *Nano-Micro Lett.* **2023**, *15*, 206; d) F. Di Giacomo, A. Fakharuddin, R. Jose, T. M. Brown, *Energy Environ. Sci.* **2016**, *9*, 3007.

[7] a) B. Du, K. Fukuda, T. Yokota, D. Inoue, D. Hashizume, S. Xiong, S. Lee, M. Takakuwa, L. Sun, J. Wang, T. Someya, *ACS Appl. Mater. Interfaces* **2023**, *15*, 14624; b) N. Lu, X. Wang, Z. Suo, J. Vlassak, *Appl. Phys. Lett.* **2007**, 91; c) S. R. Dupont, E. Voroshazi, P. Heremans, R. H. Dauskardt, *Org. Electron.* **2013**, *14*, 1262; d) L. Li, Y. Wang, X. Wang, R. Lin, X. Luo, Z. Liu, K. Zhou, S. Xiong, Q. Bao, G. Chen, Y. Tian, Y. Deng, K. Xiao, J. Wu, M. I. Saidaminov, H. Lin, C.-Q. Ma, Z. Zhao, Y. Wu, L. Zhang, H. Tan, *Nat. Energy* **2022**, *7*, 708.

[8] a) X. Zheng, L. Zuo, K. Yan, S. Shan, T. Chen, G. Ding, B. Xu, X. Yang, J. Hou, M. Shi, H. Chen, *Energy Environ. Sci.* **2023**, *16*, 2284; b) H. C. Weerasinghe, Y. Dkhissi, A. D. Scully, R. A. Caruso, Y.-B. Cheng, *Nano Energy* **2015**, *18*, 118; c) L. Sun, J. Wang, H. Matsui, S. Lee, W. Wang, S. Guo, H. Chen, K. Fang, Y. Ito, D. Inoue, D. Hashizume, K. Mori, M. Takakuwa, S. Lee, Y. Zhou, T. Yokota, K. Fukuda, T. Someya, *Sci. Adv.* **2024**, *10*, eadk9460.

[9] S. Tu, Y. Gang, Y. Lin, X. Liu, Y. Zhong, D. Yu, X. Li, *Small* **2024**, *20*, 2310868.

[10] D. Zhao, C. Zhang, J. Ren, S. Li, Y. Wu, Q. Sun, Y. Hao, *Small* **2024**, *20*, 2308364.

[11] N. Ren, L. Tan, M. Li, J. Zhou, Y. Ye, B. Jiao, L. Ding, C. Yi, *iEnergy* **2024**, *3*, 39.

[12] X. Tong, L. Xie, J. Li, Z. Pu, S. Du, M. Yang, Y. Gao, M. He, S. Wu, Y. Mai, Z. Ge, *Adv. Mater.* **2024**, *36*, 2407032.

[13] R. Xu, F. Pan, J. Chen, J. Li, Y. Yang, Y. Sun, X. Zhu, P. Li, X. Cao, J. Xi, J. Xu, F. Yuan, J. Dai, C. Zuo, L. Ding, H. Dong, A. K.-Y. Jen, Z. Wu, *Adv. Mater.* **2024**, *36*, 2308039.

[14] a) K. Fukuda, K. Yu, T. Someya, *Adv. Energy Mater.* **2020**, *10*, 2000765; b) W. Kim, I. Lee, D. Yoon Kim, Y.-Y. Yu, H.-Y. Jung, S. Kwon, W. Seo Park, T.-S. Kim, *Nanotechnology* **2017**, *28*, 194002.

[15] a) M. Ye, X. Hong, F. Zhang, X. Liu, *J. Mater. Chem. A* **2016**, *4*, 6755; b) H. S. Jung, G. S. Han, N.-G. Park, M. J. Ko, *Joule* **2019**, *3*, 1850; c) Y. Li, G. Xu, C. Cui, Y. Li, *Adv. Energy Mater.* **2018**, *8*, 1701791.

[16] K. Fukuda, L. Sun, B. Du, M. Takakuwa, J. Wang, T. Someya, L. F. Marsal, Y. Zhou, Y. Chen, H. Chen, S. R. P. Silva, D. Baran, L. A. Castriotta, T. M. Brown, C. Yang, W. Li, A. W. Y. Ho-Baillie, T. Österberg, N. P. Padture, K. Forberich, C. J. Brabec, O. Almora, *Nat. Energy* **2024**, *9*, 1335.

[17] K. Fukuda, T. Sekine, R. Shiwaku, T. Morimoto, D. Kumaki, S. Tokito, *Sci. Rep.* **2016**, *6*, 27450.

[18] Y. Leterrier, in *Handbook of Flexible Organic Electronics*, (Ed: S. Logothetidis), Woodhead Publishing, Oxford **2015**, p. 3, https://doi.org/10.1016/B978-1-78242-035-4.00001-4.

[19] D.-H. Kim, J.-H. Ahn, W. M. Choi, H.-S. Kim, T.-H. Kim, J. Song, Y. Y. Huang, Z. Liu, C. Lu, J. A. Rogers, *Science* **2008**, *320*, 507.

[20] T. Sekitani, Y. Kato, S. Iba, H. Shinaoka, T. Someya, T. Sakurai, S. Takagi, *Appl. Phys. Lett.* **2005**, 86.

[21] Z. Suo, E. Y. Ma, H. Gleskova, S. Wagner, *Appl. Phys. Lett.* **1999**, *74*, 1177.

[22] G. Lee, M.-c. Kim, Y. W. Choi, N. Ahn, J. Jang, J. Yoon, S. M. Kim, J.-G. Lee, D. Kang, H. S. Jung, M. Choi, *Energy Environ. Sci.* **2019**, *12*, 3182.

[23] N. Cui, Y. Song, C.-H. Tan, K. Zhang, X. Yang, S. Dong, B. Xie, F. Huang, *npj Flex. Electron.* **2021**, *5*, 31.

[24] P. J. Hine, A. Astruc, I. M. Ward, *J Appl. Polym. Sci.* **2004**, *93*, 796.

[25] D. Zorko, I. Demšar, J. Tavčar, *Polym. Test.* **2021**, *93*, 106994.

[26] T. Sakai, A. Nakagawa, Y. Nakamura, N. Oguma, *Appl. Sci.* **2021**, *11*, 2889.

[27] O. Almora, C. I. Cabrera, S. Erten-Ela, K. Forberich, K. Fukuda, F. Guo, J. Hauch, A. W. Y. Ho-Baillie, T. J. Jacobsson, R. A. J. Janssen, T. Kirchartz, M. A. Loi, X. Mathew, D. B. Mitzi, M. K. Nazeeruddin, U. W. Paetzold, B. P. Rand, U. Rau, T. Someya, E. Unger, L. Vaillant-Roca, C. J. Brabec, *Adv. Energy Mater.* **2024**, *14*, 2303173.

[28] F. Qin, L. Sun, H. Chen, Y. Liu, X. Lu, W. Wang, T. Liu, X. Dong, P. Jiang, Y. Jiang, L. Wang, Y. Zhou, *Adv. Mater.* **2021**, *33*, 2103017.

[29] S.-m. Ahn, E. D. Jung, S.-H. Kim, H. Kim, S. Lee, M. H. Song, J.-Y. Kim, *Nano Lett.* **2019**, *19*, 3707.

[30] B. C. Kim, J.-Y. Hong, G. G. Wallace, H. S. Park, *Adv. Energy Mater.* **2015**, *5*, 1500959.

[31] G. Zhou, F. Li, H.-M. Cheng, *Energy Environ. Sci.* **2014**, *7*, 1307.

[32] Y. Wang, L. Yang, X.-L. Shi, X. Shi, L. Chen, M. S. Dargusch, J. Zou, Z.-G. Chen, *Adv. Mater.* **2019**, *31*, 1807916.

[33] A. Sasmal, A. Arockiarajan, *Nano Energy* **2023**, *115*, 108733.

[34] Y. Wu, Y. Ma, H. Zheng, S. Ramakrishna, *Mater. Des.* **2021**, *211*, 110164.

[35] M. A. Miner, *J. Appl. Mech.* **2021**, *12*, A159.

[36] Y. Murakami, T. Takagi, K. Wada, H. Matsunaga, *Int. J. Fatigue* **2021**, *146*, 106138.

[37] L. C. Rendler, J. Walter, S. Goldenberg, A. J. Beinert, S. Wiese, U. Eitner, *Sol. Energy Mater. Sol. Cells* **2018**, *176*, 204.

[38] C. Hengst, S. B. Menzel, G. K. Rane, V. Smirnov, K. Wilken, B. Leszczynska, D. Fischer, N. Prager, *Materials* **2017**, *10*, 245.

[39] M. Kim, B.-U. Moon, C. H. Hidrovo, *J. Micromech. Microeng.* **2013**, *23*, 095024.

[40] S. Lee, J.-Y. Kwon, D. Yoon, H. Cho, J. You, Y. T. Kang, D. Choi, W. Hwang, *Nanoscale Res. Lett.* **2012**, *7*, 256.

[41] a) Y. Leterrier, L. Médico, F. Demarco, J. A. E. Månson, U. Betz, M. F. Escolà, M. Kharrazi Olsson, F. Atamny, *Thin Solid Films* **2004**, *460*, 156; b) K. Zeng, F. Zhu, J. Hu, L. Shen, K. Zhang, H. Gong, *Thin Solid Films* **2003**, *443*, 60.

[42] J.-W. Jiang, J.-S. Wang, B. Li, *Phys. Rev. B* **2009**, *80*, 113405.

[43] X. Duan, Y. Ding, R. Liu, *Mater. Today Energy* **2023**, *37*, 101409.

[44] J. Qu, L. Ouyang, C.-c. Kuo, D. C. Martin, *Acta Biomater.* **2016**, *31*, 114.

[45] M. M. Tavakoli, Q. Lin, S.-F. Leung, G. C. Lui, H. Lu, L. Li, B. Xiang, Z. Fan, *Nanoscale* **2016**, *8*, 4276.

[46] D. A. Dikin, S. Stankovich, E. J. Zimney, R. D. Piner, G. H. B. Dommett, G. Evmenenko, S. T. Nguyen, R. S. Ruoff, *Nature* **2007**, *448*, 457.

[47] H. N. Yoshimura, A. L. Molisani, N. E. Narita, J. L. A. Manholetti, J. M. Cavenaghi, *Mater. Sci. Forum* **2006**, *530–531*, 408.

[48] R. Gaillac, P. Pullumbi, F.-X. Coudert, *J. Phys. Condens. Mat.* **2016**, *28*, 275201.
[49] a) J. M. Méndez-Hernández, A. Hernández-Pérez, M. Oviedo-Mendoza, E. Hernández-Rodríguez, *Mech. Mater.* **2021**, *154*, 103708; b) D. J. Lipomi, H. Chong, M. Vosgueritchian, J. Mei, Z. Bao, *Sol. Energy Mater Sol. Cells* **2012**, *107*, 355.
[50] C. Yan, J. Qin, Y. Wang, G. Li, P. Cheng, *Adv. Energy Mater.* **2022**, *12*, 2201087.
[51] J.-W. Lee, B. S. Ma, H. J. Kim, T.-S. Kim, B. J. Kim, *JACS Au* **2021**, *1*, 612.
[52] a) Q. Tu, D. Kim, M. Shyikh, M. G. Kanatzidis, *Matter* **2021**, *4*, 2765; b) D. B. Kim, J. W. Lee, Y. S. Cho, *Adv. Funct. Mater.* **2021**, *31*, 2007131.
[53] J. Moghal, H. Suttle, A. G. Cook, C. R. M. Grovenor, H. E. Assender, *Surf. Coat. Tech.* **2012**, *206*, 3309.
[54] S. Rühle, *Solar Energy* **2016**, *130*, 139.